End-to-end interpretable learning of non-blind image deblurring - supplemental material

Anonymous ECCV submission

Paper ID 2749

1 Additional non-uniform deblurring quantitative results

The results reported in our submission for non-uniform blur are only for 1% additive white Gaussian noise. We show below (Table 1) for completness the results for 1%, 3% and 5% noise levels. The experimental protocol and code used in these experiments are exactly the same as in the main paper. The test dataset is the non-uniform PASCAL benchmark presented in our submission. The proposed (L)CHQS models embed 5 outer HQS iterations and 2 inner CPCR iterations. The table shows that our method outperforms its competitors for all noise levels, with, in particular, a very significant margin of about 0.9dB with LCHQS_F over HQS-CG and EPLL [9].

	HQS-FFT	HQS-CG	EPLL	CHQS	LCHQS_G	LCHQS_F
1% noise	23.49 ± 0.09	25.84 ± 0.08	25.49 ± 0.08	25.11 ± 0.10	26.83 ± 0.08	**26.98 ± 0.08**
3% noise	23.17 ± 0.07	24.18 ± 0.06	23.78 ± 0.05	23.74 ± 0.07	24.91 ± 0.05	**25.06 ± 0.06**
5% noise	22.44 ± 0.06	23.10 ± 0.05	23.34 ± 0.06	22.65 ± 0.06	23.97 ± 0.05	**24.14 ± 0.05**

Table 1: Non-uniform blur removal results with 1%, 3% and 5% additive Gaussian noise on the non-uniform PASCAL benchmark of 100 blurry images.

2 Derivation of the expression for the filters c_i in Eq. (11)

We intend to solve Eq. (10) in the main paper:

$$\min_C \|\delta - C \star L\|_F^2 + \rho \sum_{i=0}^{n} \|c_i\|_F^2.$$

Using the Parseval identity, this becomes, in the Fourier domain:

$$\min_{\tilde{C}} \|J - \tilde{C} \odot \tilde{L}\|_F^2 + \rho \sum_{i=0}^{n} \|\tilde{C}_i\|_F^2, \tag{1}$$

where $\tilde{L}$, $\tilde{C}$ and the $\tilde{C}_i$'s are the Fourier transforms of L, C and the c_i filters ($i = 0, \ldots, n$), J is the matrix full of ones and $\odot$ is the entrywise product.

Now we compute the gradient of this energy with respect to each filter $\tilde{C}_i$ at the minimum. By denoting by $\tilde{K}_i$ the Fourier transform of the filter k_i (with $k_0 = k$) for i in $[0, \dots, n]$, we use the equalities $\tilde{C} \odot \tilde{L} = \tilde{L} \odot \tilde{C} = \sum_{j=0}^{n} \tilde{K}_j \odot \tilde{C}_j$, by definition of the c_j's in Eq. (9) of the submission, to compute the derivative with respect to each $\tilde{C}_i$ of Eq. (1)

$$0 = \tilde{K}_i^* \odot \left(J - \sum_{j=0}^{n} \tilde{K}_j \odot \tilde{C}_j \right) - \rho \tilde{C}_i,$$

where $\tilde{K}_i^*$ is the complex conjugate of $\tilde{K}_i$. The Fourier transform $\tilde{C}_i$ of each filter c_i verifies

$$\rho \tilde{C}_i = \tilde{K}_i^* \odot \left(J - \sum_{j=0}^{n} \tilde{K}_j \odot \tilde{C}_j \right). \tag{2}$$

We now seek to obtain an expression of $\sum_{j=0}^{n} \tilde{K}_j \odot \tilde{C}_j$ independent of the $\tilde{C}_i$'s in order to make Eq. (2) depending only on the unknown filter $\tilde{C}_i$, for all i in $[0, \dots, n]$. To do so, we multiply both sides of Eq. (2) by $\tilde{K}_i$ $(i = 0, \dots, n)$ and get:

$$\rho \tilde{K}_i \odot \tilde{C}_i = |\tilde{K}_i|^2 \odot \left(J - \sum_{j=0}^{n} \tilde{K}_j \odot \tilde{C}_j \right), \tag{3}$$

where $|\tilde{K}_i|^2$ is the matrix whose entries are the square moduli of the entries of $\tilde{K}_i$. Summing for all i in $[0, \dots, n]$ Eq. (3) gives

$$\rho \sum_{j=0}^{n} \tilde{K}_j \odot \tilde{C}_j = \left(\sum_{j=0}^{n} |\tilde{K}_j|^2 \right) \odot \left(J - \sum_{j=0}^{n} \tilde{K}_j \odot \tilde{C}_j \right),$$

or, after rearranging terms

$$\sum_{j=0}^{n} \tilde{K}_j \odot \tilde{C}_j = \frac{\sum_{j=0}^{n} |\tilde{K}_j|^2}{\rho J + \sum_{j=0}^{n} |\tilde{K}_j|^2},$$

where the division is entrywise in the Fourier domain. We now have an expression of $\sum_{j=0}^{n} \tilde{K}_j \odot \tilde{C}_j$ independent from the $\tilde{C}_j$'s. Plugging it into Eq. (2) yields, for all i in $[0, \dots, n]$

$$\rho \tilde{C}_i = \tilde{K}_i^* \odot \left(J - \frac{\sum_{j=0}^{n} |\tilde{K}_j|^2}{\rho J + \sum_{j=0}^{n} |\tilde{K}_j|^2} \right). \tag{4}$$

Because multiplications and divisions are entrywise in this context, we can write J as

$$J = \frac{\rho J + \sum_{j=0}^{n} |\tilde{K}_j|^2}{\rho J + \sum_{j=0}^{n} |\tilde{K}_j|^2}.$$

Injecting this expression in Eq. (4) finally gives

$$\begin{aligned}\tilde{C}_i &= \frac{1}{\rho}\tilde{K}_i^* \odot \left(\frac{\rho J + \sum_{j=0}^n |\tilde{K}_j|^2}{\rho J + \sum_{j=0}^n |\tilde{K}_j|^2} - \frac{\sum_{j=0}^n |\tilde{K}_j|^2}{\rho J + \sum_{j=0}^n |\tilde{K}_j|^2} \right) \\ &= \frac{\tilde{K}_i^*}{\rho J + \sum_{j=0}^n |\tilde{K}_j|^2}.\end{aligned}$$

Finally, each optimal filter c_i is the inverse Fourier transform of the corresponding $\tilde{C}_i$, as stated in Eq. (11) of our submission.

3 Computation of the spectral radius of Id-$[L]_\star[C]_\star$

The filters k_j (j in $[0, \dots, n]$) have size $w_k \times w_k$, the $n+1$ corresponding approximate inverse filters c_j have size $w_c \times w_c$. Thus, the Dirac filter δ in Eq. (10) of our submission has size $(w_c - w_k + 1) \times (w_c - w_k + 1)$ for a "valid" convolution, *i.e.,* a convolution without (zero) padding.

The linear operator $[L]_\star$ associated with L (a horizontal stack of circulant matrices) has size $m \times [(n+1)p]$ and the linear operator $[C]_\star$ (a vertical stack of circulant matrices) has size $[(n+1)p] \times m$ with $m = (w_c - w_k + 1)^2$ and $p = w_c^2$. Thus $H = \mathrm{Id} - [L]_\star [C]_\star$, the iteration matrix in CPCR, has size $m \times m$.

Now that we have defined the dimensions of H, we compute its spectrum. Let $[L]_\star = U\Sigma V^\top$ be the singular value decomposition of $[L]_\star$ with singular values σ_i ($i = 1, \dots, m$). The singular values are all strictly positive because each filter k_j corresponds to a circulant matrix that is full-rank. The solution of Eq. (10) is the (regularized) pseudoinverse of $[L]_\star$ (see Golub and Van Loan [1], Sec. 6.1.4):

$$[C]_\star = V(\Sigma + \rho\Sigma^{-1})^{-1}U^\top.$$

Thus, we can rewrite H as follows

$$\begin{aligned}H &= \mathrm{Id} - [L]_\star[C]_\star, \\ &= \mathrm{Id} - U(\Sigma + \rho\Sigma^{-1})^{-1}\Sigma U^\top, \\ &= U\mathrm{Diag}(1 - \sigma_1^2/(\rho + \sigma_1^2), \dots, 1 - \sigma_n^2/(\rho + \sigma_n^2))U^\top, \\ &= U\mathrm{diag}(\lambda_1, \dots, \lambda_n)U^\top,\end{aligned}$$

with $\lambda_i = \rho/(\rho + \sigma_i^2) < 1$ for all i in $[1, \dots, m]$ since $\rho > 0$. Thus, the spectral radius of H is $\rho/(\rho + \min_i \sigma_i^2)$ and is strictly smaller than 1, meaning that CPCR converges linearly thanks to the properties of Richardson iterations (see Kelley [3], Sec 1.2).

4 Empirical spectral radius of H

In this section, we compute the empirical eigenvalues of the operator $H^\top H$ for the 8 kernels provided by Levin *et al.* [5]. We compute the linear operator $[C]_\star$

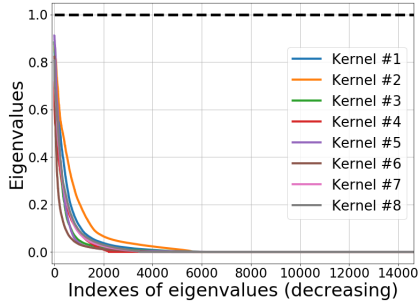

Fig. 1: Eigenvalues of $H^\top H$ for the 8 kernels of Levin *et al.*

by solving Eq. (10) with $n = 1$ (*i.e.*, $\lambda = 0$ in Eq. (9)) and $\rho = 0.05$. We set $w_k + w_c - 1 = 121$ for the 8 kernels with different sizes $w_k \times w_k$ (varying between 13×13 and 27×27), so $H^\top H$ is a 14641×14641 matrix.

Figure 1 shows the eigenvalues of $H^\top H$ for the 8 blur kernels in the Levin dataset. As expected from the previous section, all the eigenvalues are below 1, thus the spectral radius of H is smaller than 1.

5 Additional deblurring results

We present below additional qualitative results with images sampled from the Levin [5], Sun [7] and Pascal datasets, with various amounts of noise. Concretely, Figures 2 and 3 show additional results on the Levin dataset for uniform blur with 0.5% noise. Figures 5 and 6 show results on the Sun dataset for uniform blur with 1% noise. Figures 7 to 12 show results on the Pascal dataset for uniform blur and noise levels varying from 1 to 5%. Figures 13 to 18 show results on the Pascal dataset for *non-uniform* blur with noise levels varying from 1 to 5%. These images are better seen on a computer screen. The PSNR scores for each image are in parentheses.

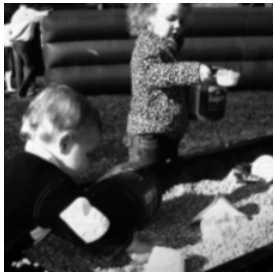

(a) Ground truth.

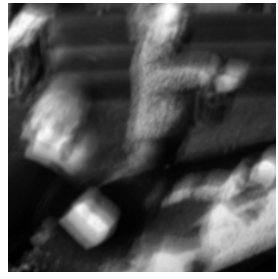

(b) Blurry image.

(c) EPLL [9] (31.47 dB).

(d) FCNN [8] (31.26 dB).

(e) FDN [4] (33.70 dB).

(f) Ours (33.31 dB).

Fig. 2: Comparison of our method with EPLL [9], FCNN [8] and FDN [4] on an image from the Levin dataset [5] with 0.5% noise.

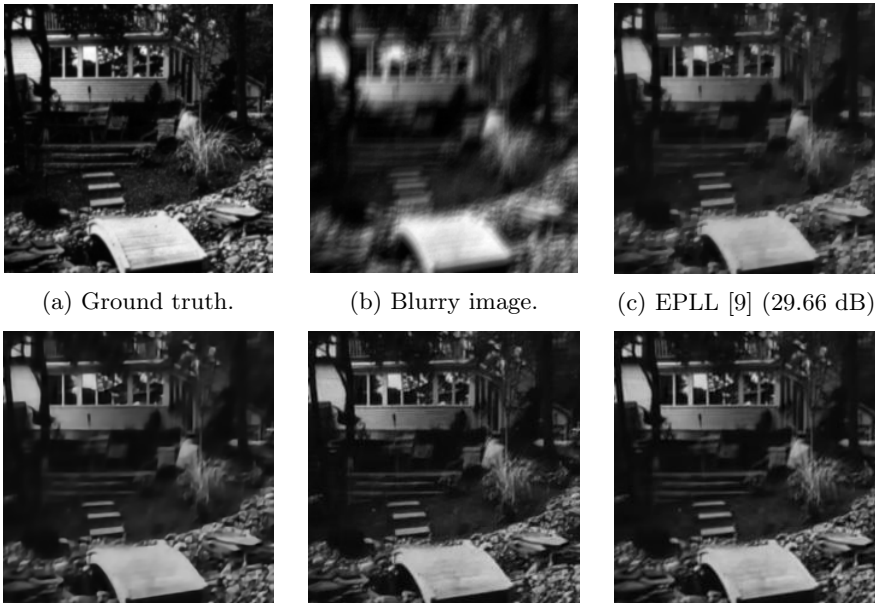

(a) Ground truth. (b) Blurry image. (c) EPLL [9] (29.66 dB).

(d) FCNN [8] (31.78 dB). (e) FDN [4] (33.83 dB). (f) Ours (33.93 dB).

Fig. 3: Comparison of our method with EPLL [9], FCNN [8] and FDN [4] on an image from the Levin dataset [5] with 0.5% noise.

(a) Ground truth.

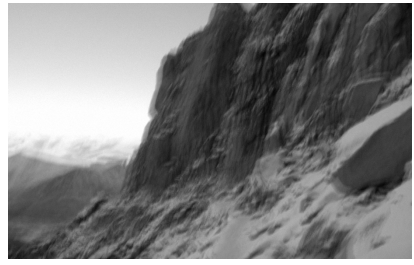

(b) Blurry image.

(c) EPLL [9] (31.66 dB).

(d) FCNN [8] (31.55 dB).

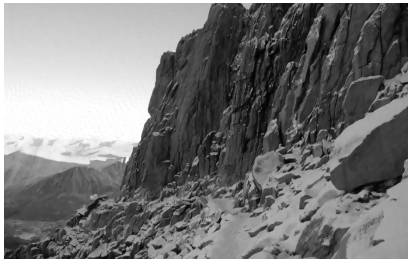

(e) FDN [4] (31.74 dB).

(f) Ours (31.76 dB).

Fig. 4: Comparison of our method with EPLL [9], FCNN [8] and FDN [4] on an image from the Sun dataset [7] with 1% noise.

(a) Ground truth.

(b) Blurry image.

(c) EPLL [9] (33.62 dB).

(d) FCNN [8] (33.67 dB).

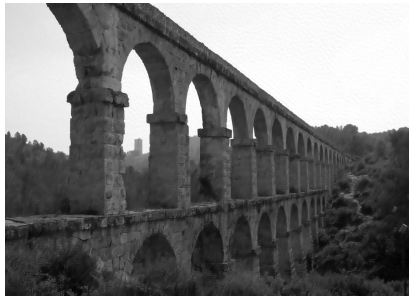

(e) FDN [4] (33.67 dB).

(f) Ours (34.05 dB).

Fig. 5: Comparison of our method with EPLL [9], FCNN [8] and FDN [4] on an image from the Sun dataset [7] with 1% noise.

(a) Ground truth.

(b) Blurry image.

(c) EPLL [9] (33.12 dB).

(d) FCNN [8] (32.99 dB).

(e) FDN [4] (33.62 dB).

(f) Ours (34.03 dB).

Fig. 6: Comparison of our method with EPLL [9], FCNN [8] and FDN [4] on an image from the Sun dataset [7] with 1% noise.

(a) Ground truth.

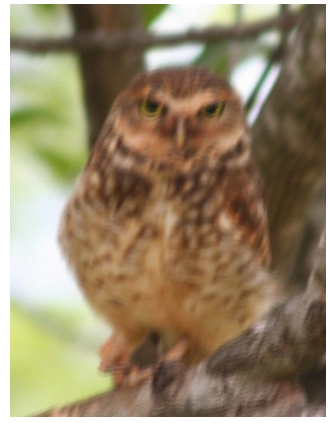

(b) Blurry image.

(c) EPLL [9] (32.50 dB).

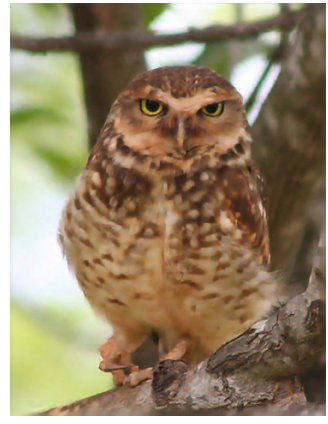

(d) FCNN [8] (32.43 dB).

(e) FDN [4] (32.36 dB).

(f) Ours (32.90 dB).

Fig. 7: Comparison of our method with EPLL [9], FCNN [8] and FDN [4] on an image from PASCAL VOC dataset blurred with a kernel from [5] with 1% noise.

(a) Ground truth.

(b) Blurry image.

(c) EPLL [9] (26.43 dB).

(d) FCNN [8] (25.31 dB).

(e) FDN [4] (26.75 dB).

(f) Ours (27.31 dB).

Fig. 8: Comparison of our method with EPLL [9], FCNN [8] and FDN [4] on an image from PASCAL VOC dataset blurred with a kernel from [5] with 1% noise.

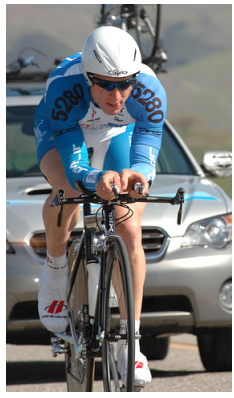

(a) Ground truth.

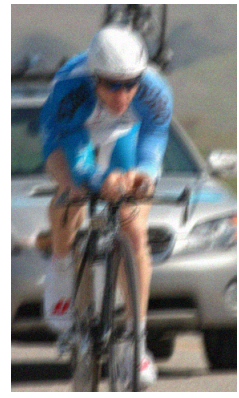

(b) Blurry image.

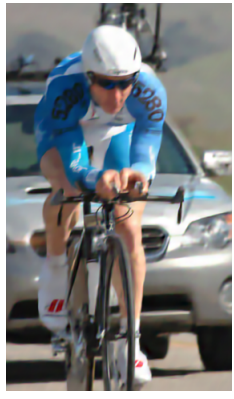

(c) EPLL [9] (23.45 dB).

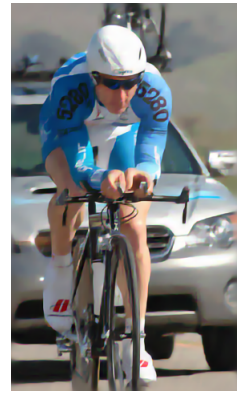

(d) FCNN [8] (25.85 dB).

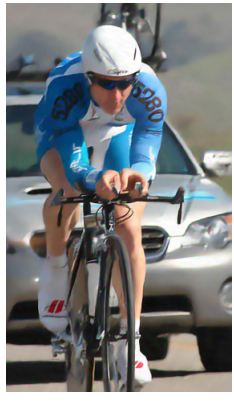

(e) FDN [4] (25.54 dB).

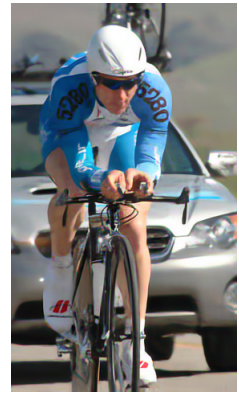

(f) Ours (25.71 dB).

Fig. 9: Comparison of our method with EPLL [9], FCNN [8] and FDN [4] on an image from PASCAL VOC dataset blurred with a kernel from [5] with 3% noise.

(a) Ground truth.

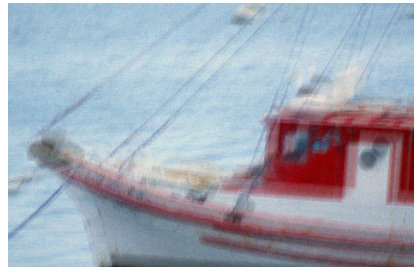

(b) Blurry image.

(c) EPLL [9] (21.91 dB).

(d) FCNN [8] (22.83 dB).

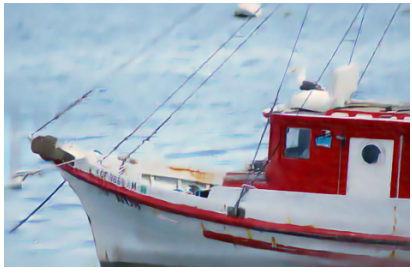

(e) FDN [4] (23.02 dB).

(f) Ours (23.53 dB).

Fig. 10: Comparison of our method with EPLL [9], FCNN [8] and FDN [4] on an image from PASCAL VOC dataset blurred with a kernel from [5] with 3% noise.

(a) Ground truth. (b) Blurry image.

(c) EPLL [9] (23.95 dB). (d) FCNN [8] (25.46 dB).

(e) FDN [4] (25.92 dB). (f) Ours (25.95 dB).

Fig. 11: Comparison of our method with EPLL [9], FCNN [8] and FDN [4] on an image from PASCAL VOC dataset blurred with a kernel from [5] with 5% noise.

(a) Ground truth.

(b) Blurry image.

(c) EPLL [9] (16.75 dB).

(d) FCNN [8] (17.72 dB).

(e) FDN [4] (18.61 dB).

(f) Ours (18.54 dB).

Fig. 12: Comparison of our method with EPLL [9], FCNN [8] and FDN [4] on an image from PASCAL VOC dataset blurred with a kernel from [5] with 5% noise.

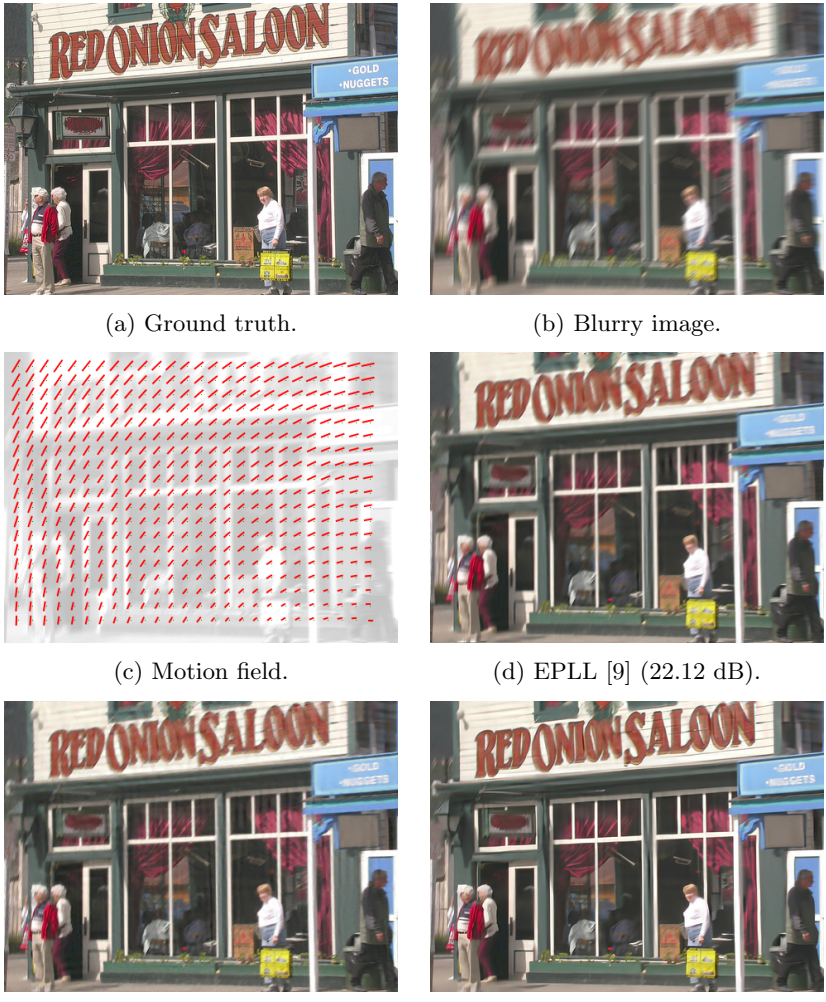

(a) Ground truth. (b) Blurry image.

(c) Motion field. (d) EPLL [9] (22.12 dB).

(e) HQS-CG (22.54 dB). (f) Ours (23.44 dB).

Fig. 13: Comparison of our method with EPLL [9] (modified by [6] for the non-uniform case) and HQS-CG on an image from PASCAL VOC dataset blurred with a motion blur synthesized with the code of [2] with 1% noise.

(a) Ground truth.

(b) Blurry image.

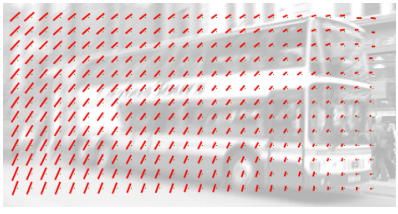

(c) Motion field.

(d) EPLL [9] (22.59 dB).

(e) HQS-CG (22.82 dB).

(f) Ours (24.00 dB).

Fig. 14: Comparison of our method with EPLL [9] (modified by [6] for the non-uniform case) and HQS-CG with 1% noise.

(a) Ground truth.

(b) Blurry image.

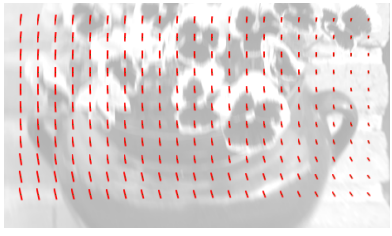

(c) Motion field.

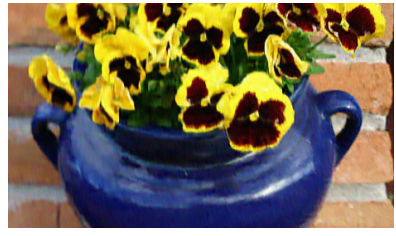

(d) EPLL [9] (24.08 dB).

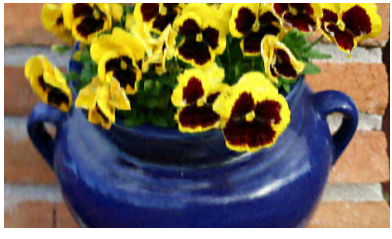

(e) HQS-CG (24.51 dB).

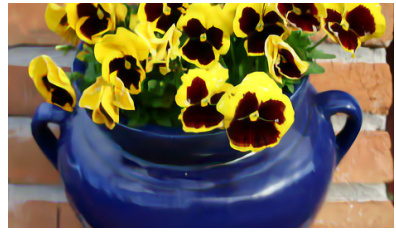

(f) Ours (25.77 dB).

Fig. 15: Comparison of our method with EPLL [9] (modified by [6] for the non-uniform case) and HQS-CG with 3% noise.

(a) Ground truth.

(b) Blurry image.

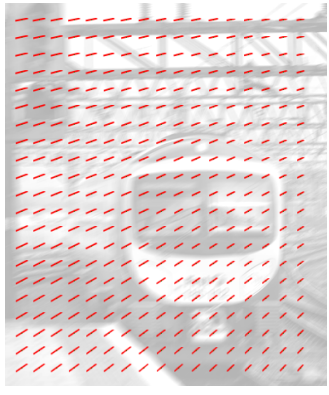

(c) Motion field.

(d) EPLL [9] (18.65 dB).

(e) HQS-CG (18.90 dB).

(f) Ours (19.87 dB).

Fig. 16: Comparison of our method with EPLL [9] (modified by [6] for the non-uniform case) and HQS-CG with 3% noise.

(a) Ground truth.

(b) Blurry image.

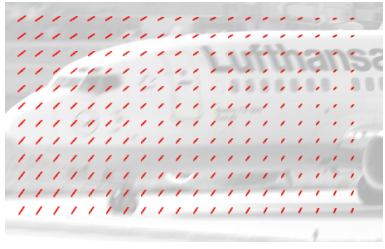

(c) Motion field.

(d) EPLL [9] (22.96 dB).

(e) HQS-CG (22.89 dB).

(f) Ours (23.05 dB).

Fig. 17: Comparison of our method with EPLL [9] (modified by [6] for the non-uniform case) and HQS-CG with 5% noise.

(a) Ground truth.

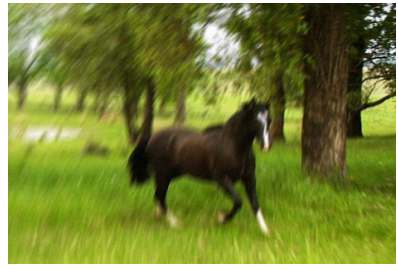

(b) Blurry image.

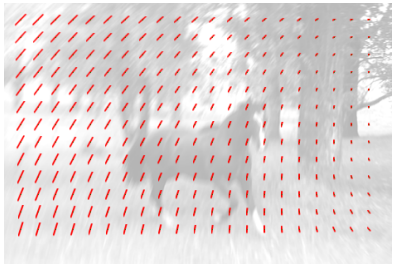

(c) Motion field.

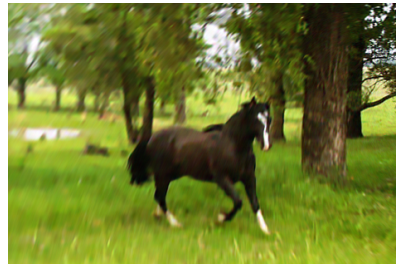

(d) EPLL [9] (23.21 dB).

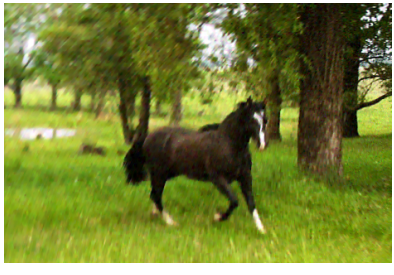

(e) HQS-CG (22.74 dB).

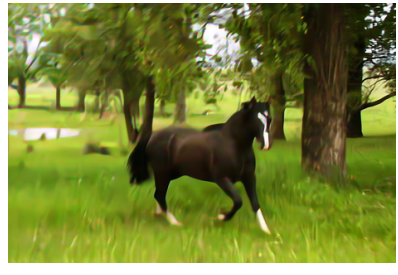

(f) Ours (24.34 dB).

Fig. 18: Comparison of our method with EPLL [9] (modified by [6] for the non-uniform case) and HQS-CG with 5% noise.

References

1. Golub, G.H., Van Loan, C.F.: Matrix computations (4th ed.). John Hopkins University Press (2013)
2. Gong, D., Yang, J., Liu, L., Zhang, Y., Reid, I.D., Shen, C., van den Hengel, A., Shi, Q.: From motion blur to motion flow: A deep learning solution for removing heterogeneous motion blur. In: Proceedings of the Conference on Computer Vision and Pattern Recognition (CVPR) (2017)
3. Kelley, C.: Iterative Methods for Linear and Nonlinear Equations. SIAM (1995)
4. Kruse, J., Rother, C., Schmidt, U.: Learning to push the limits of efficient FFT-based image deconvolution. In: Proceedings of the International Conference on Computer Vision (ICCV) (2017)
5. Levin, A., Weiss, Y., Durand, F., Freeman, W.T.: Understanding and evaluating blind deconvolution algorithms. In: Proceedings of the Conference on Computer Vision and Pattern Recognition (CVPR) (2009)
6. Sun, J., Cao, W., Xu, Z., Ponce, J.: Learning a convolutional neural network for non-uniform motion blur removal. In: Proceedings of the Conference on Computer Vision and Pattern Recognition (CVPR) (2015)
7. Sun, L., Cho, S., Wang, J., Hays, J.: Edge-based blur kernel estimation using patch priors. In: Proceedings of International Conference on Computational Photography (ICCP) (2013)
8. Zhang, J., Pan, J., Lai, W., Lau, R.W.H., Yang, M.: Learning fully convolutional networks for iterative non-blind deconvolution. In: Proceedings of the Conference on Computer Vision and Pattern Recognition (CVPR) (2017)
9. Zoran, D., Weiss, Y.: From learning models of natural image patches to whole image restoration. In: Proceedings of the International Conference on Computer Vision (ICCV) (2011)